Wavelet-based Faraday Rotation Measure Synthesis

(funded by RFBR & DFG)

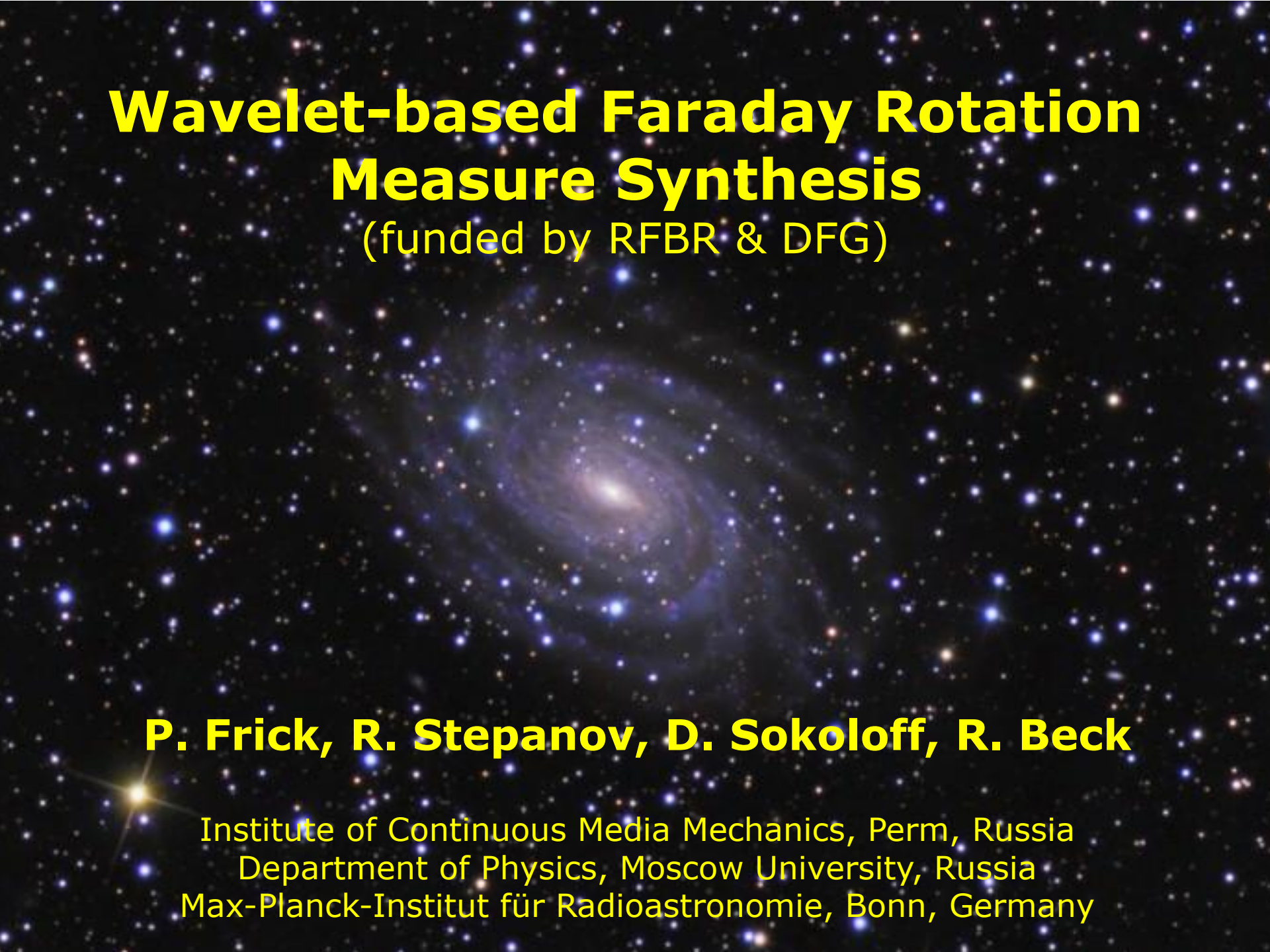

P. Frick, R. Stepanov, D. Sokoloff, R. Beck

Institute of Continuous Media Mechanics, Perm, Russia
Department of Physics, Moscow University, Russia
Max-Planck-Institut für Radioastronomie, Bonn, Germany

Standard RM Synthesis

(Frick et al., MNRAS 401, L24 (2010))

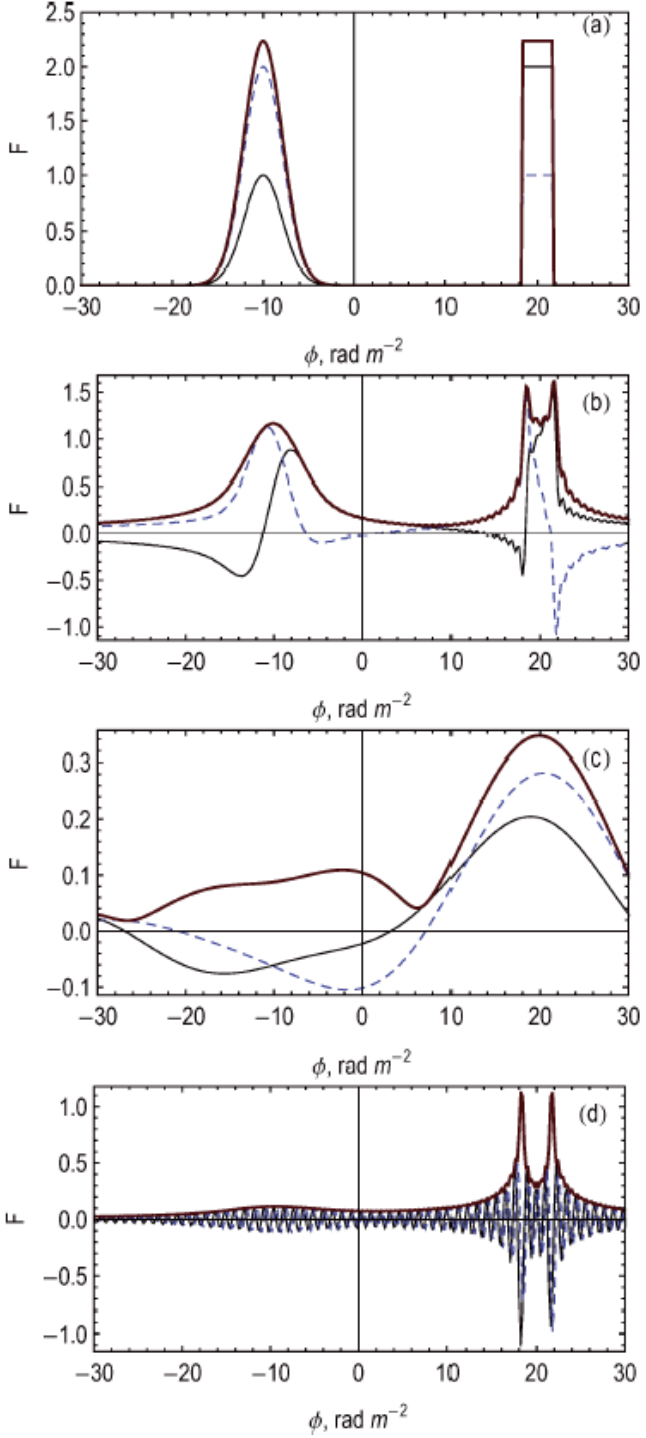

Artificial structures in Faraday space: Gaussian and box-like

Thick line: amplitude
Thin line: real part
Dashed line: imaginary part (polarisation angle)

- Box structures in Φ appear as double horns for wide spectral windows (Fig b and d)
- Gaussian structure more difficult to reconstruct
- Wrong phases (polarisation angle) for narrow **and** wide spectral windows (Fig b – d)

Figure 2. Standard RM Synthesis for a test Faraday dispersion function. (a) Original test function which includes one Gaussian and one box structure. Reconstructions: (b) using the whole domain $\lambda^2 > 0$; (c) using the window $0.6 < \lambda < 0.78$ m; (d) using the window $0.6 < \lambda < 2.5$ m. Real part – thin solid, imaginary part – dashed, amplitude – thick solid.

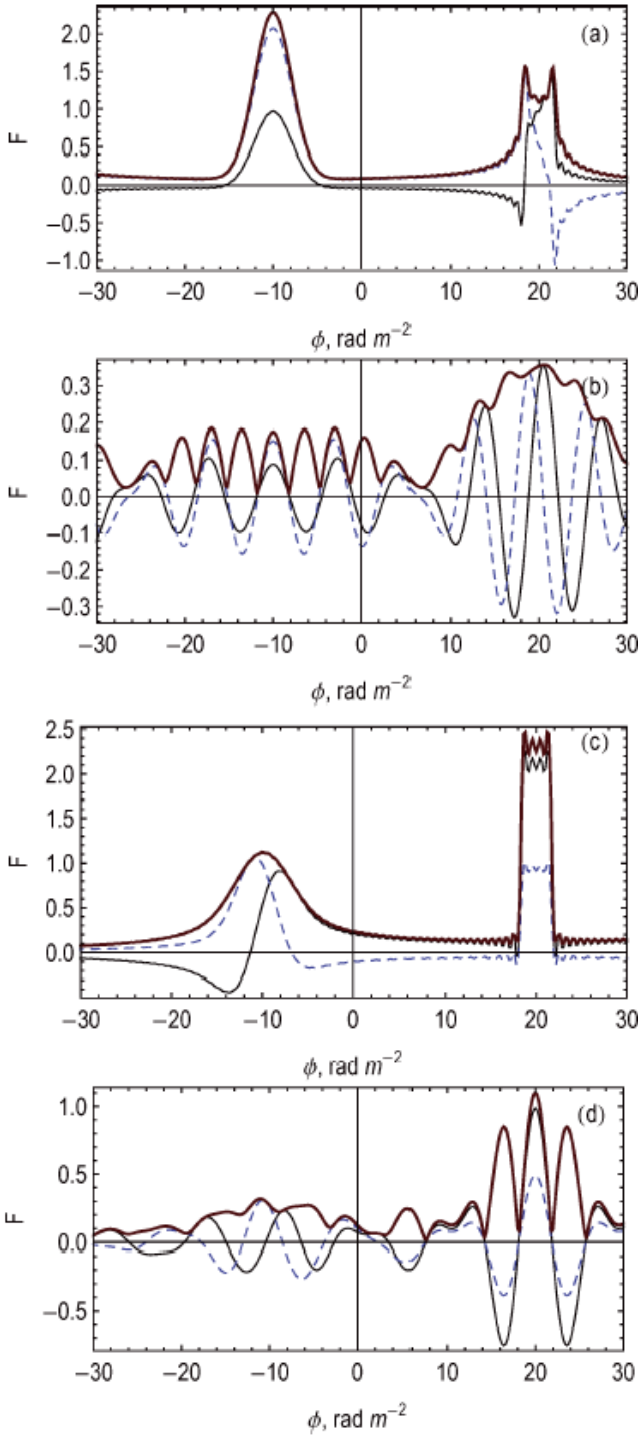

Improving the algorithm by symmetry arguments

(Frick et al. 2010)

Object is symmetric with respect to the point ϕ_0

$$F(2\phi_0 - \phi) = F(\phi)$$

then

$$P(-\lambda^2) = \exp(-4i\phi_0\lambda^2)P(\lambda^2)$$

- Excellent reconstruction of phase of **one** structure for wide spectral windows (Fig a and c)
- Good reconstruction of phase of **one** structure for narrow spectral windows (Fig b and d)

Figure 3. RM Synthesis for the test from Fig. 2 using the extension of $P(\lambda^2)$ in the domain $\lambda^2 < 0$ defined by (7). The parameter ϕ_0 is adjusted to the position of the left structure (a and b) or right structure (c and d). The whole domain of λ is used in panels (a and c) and the spectral window $0.6 < \lambda < 0.78$ m in panels (b and d). Real part – thin solid, imaginary part – dashed, amplitude – thick solid.

RM Synthesis and wavelets

(Frick et al. 2010)

Wavelet transform (direct and inverse):

$$w_{\mathrm{F}}(a,b) = \frac{1}{|a|}\int_{-\infty}^{\infty} F(\phi)\psi^*\left(\frac{\phi-b}{a}\right)\mathrm{d}\phi$$

$$F(\phi) = \frac{1}{C_\psi}\int_{-\infty}^{\infty}\int_{-\infty}^{\infty}\psi\left(\frac{\phi-b}{a}\right) w_{\mathrm{F}}(a,b)\,\frac{\mathrm{d}a\,\mathrm{d}b}{a^2}$$

Symmetry argument in wavelet space:

$$w_{\mathrm{F}}(a,b) = w_-(a,b) + w_+(a,b)$$

$$w_-(a,b) = \frac{1}{\pi}\int_{-\infty}^{0} P(\lambda^2)\mathrm{e}^{-2\mathrm{i}b\lambda^2}\hat{\psi}^*(-2a\lambda^2)\mathrm{d}\lambda^2$$

$$w_+(a,b) = \frac{1}{\pi}\int_{0}^{\infty} P(\lambda^2)\mathrm{e}^{-2\mathrm{i}b\lambda^2}\hat{\psi}^*(-2a\lambda^2)\mathrm{d}\lambda^2$$

$$w_-(a,b) = w_+\left[a, 2\phi_0^i(a,b) - b\right]$$

RM Spread Function: $R(\phi) = K \int_{-\infty}^{\infty} W(\lambda^2) e^{-2i\phi\lambda^2} d\lambda^2,$

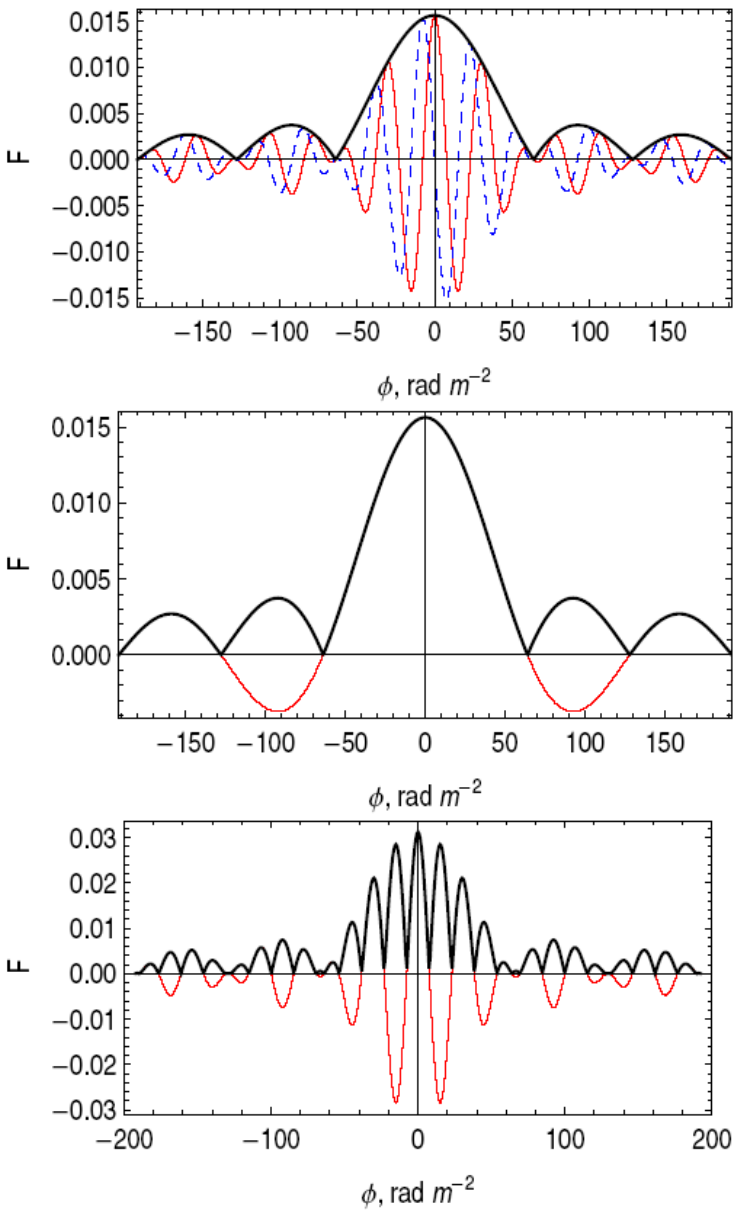

where $W(\lambda^2)$ is the shape of the observable window

Standard:

$$R(\phi) = K e^{-2i\phi\lambda_0^2} \frac{\sin(\phi\Delta\lambda^2)}{\phi}$$

$$\tilde{F}(\phi) = F(\phi) \star R(\phi)$$

B&B:

$$R_{BB}(\phi) = K \int_{-\infty}^{\infty} W(\lambda^2) e^{-2i\phi(\lambda^2-\lambda_0^2)} d\lambda^2 = K \frac{\sin(\phi\Delta\lambda^2)}{\phi}$$

$$\tilde{F}(\phi) = e^{-2i\phi\lambda_0^2} F(\phi) \star R_{BB}(\phi)$$

Wavelet:

$$R_W(\phi) = 2K \frac{\sin(\phi\Delta\lambda^2)}{\phi} \cos(2\phi\lambda_0^2)$$

$$\tilde{F}(\phi) = e^{-4i\phi_0\lambda_0^2} F(\phi) \star R_W(\phi)$$

Figure 3. RM spread functions for $\lambda_0^2 = 0.1$ and $\Delta\lambda^2 = 0.05$, m^2: (a) standard R, (b) R_{BB} and (c) R_W. Real part (thin solid red), imaginary part (dashed blue), modulus (thick black).

Wavelet-based RM Synthesis

Frick et al. 2010

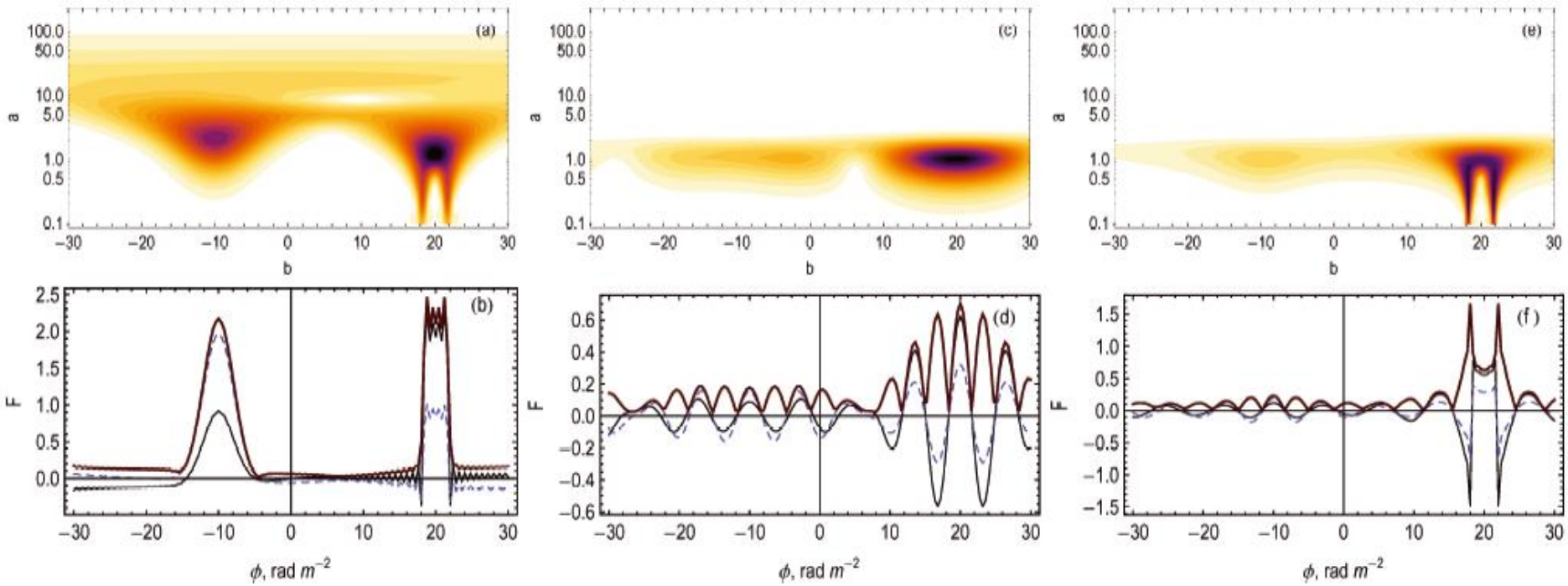

Figure 4. Wavelet-based RM Synthesis for the test from Fig. 2. The modulus of wavelet coefficients on the (a, b) plane (panels a, c and e) and the result of reconstruction (panels b, d and f) for whole domain of λ (panels a and b) and the windows $0.6 < \lambda < 0.78$ m (panels c and d) and $0.6 < \lambda < 2.5$ m (panels e and f). Real part – thin solid, imaginary part – dashed, amplitude – thick solid.

- Good reconstruction of amplitude and phase of **both** structures for narrow spectral windows (Fig c and d)

- Excellent reconstruction of amplitude and phase of **both** structures for wide spectral windows (Fig e and f)

Models of regular magnetic fields and corresponding PI and Faraday spectra

(Frick et al., MNRAS 414, 2540 (2011))

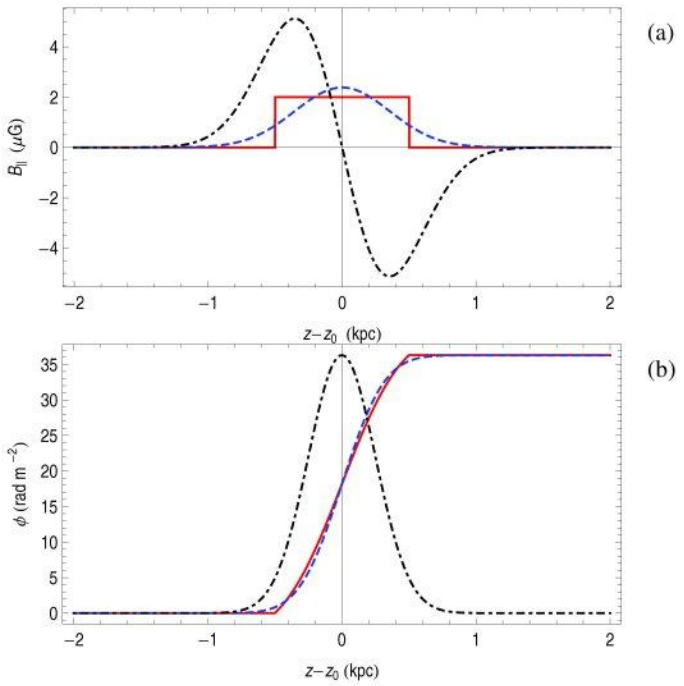

Figure 4. Typical shapes of magnetic field distribution (a): B_1 (solid line, red), B_2 (dashed, blue), B_3 (dot-dashed, black) and (b) corresponding Faraday depths ϕ.

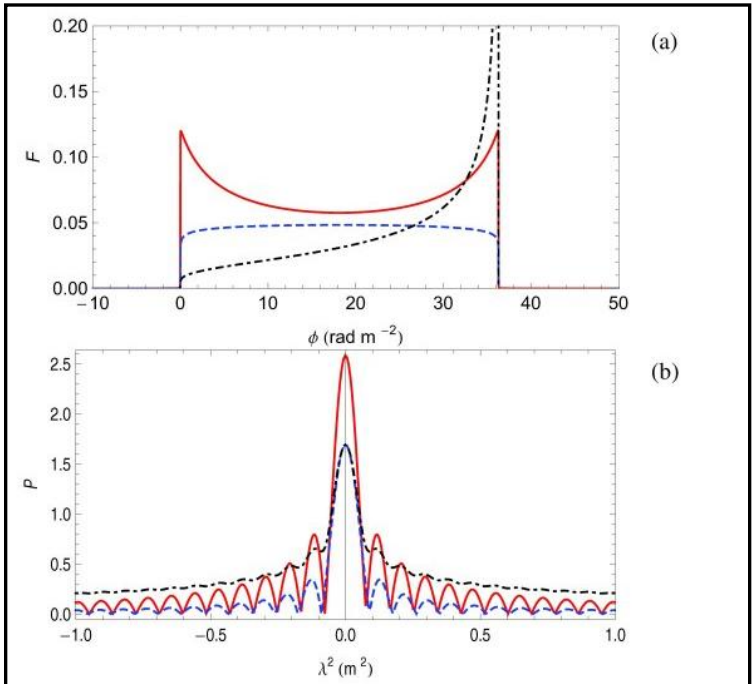

Figure 5. Real part of the Faraday dispersion function $F(\phi)$ (panel a), Im $F = 0$, and the modulus of corresponding $P(\lambda^2)$ (panel b) for different magnetic field profiles: B_1 (solid line, red), B_2 (dashed, blue), B_3 (dot-dashed, black).

Magnetic field models and Faraday depths

Faraday dispersion function and polarisation spectrum

Wavelet transform of Faraday structures by regular + turbulent magnetic fields

(Frick et al. 2011)

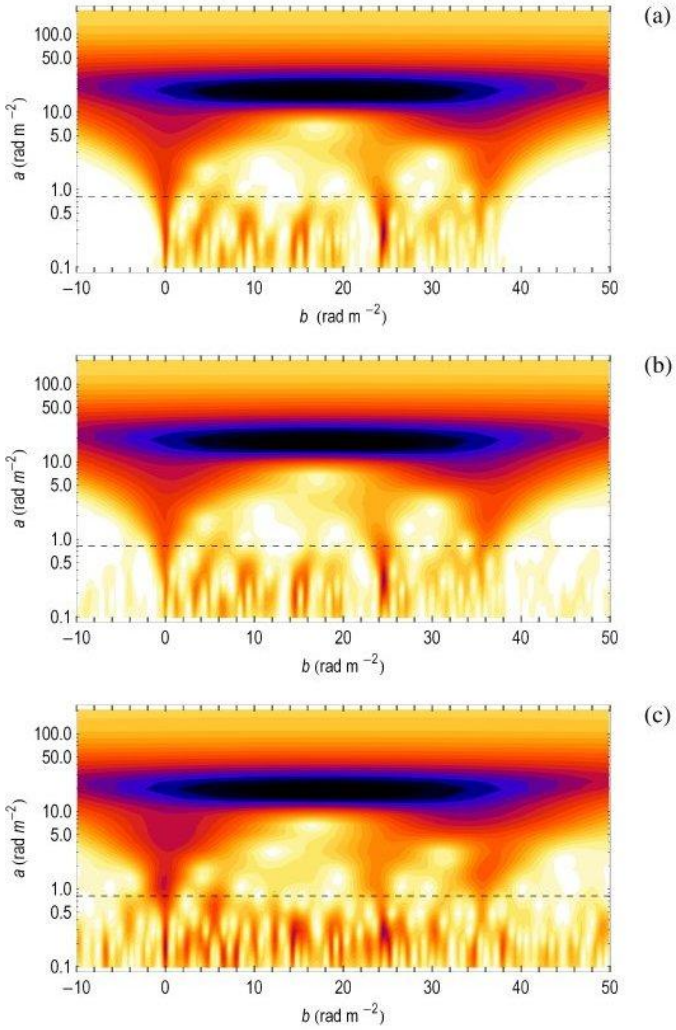

Figure 11. Wavelet plane $w_F(a, b)$ calculated for different ratios of signal-to-noise from $P(\lambda^2)$, obtained for the wide beam (shown in Fig. 10b by the black line). From top to bottom: signal without noise, signal-to-noise ratios of 2 and 0.5. The horizontal dashed line shows the upper bound of the domain admissible to LOFAR-type observations.

No noise

Signal/noise = 2

Signal/noise = 0.5

Horizontal dashed line:
λ = 1.25 – 2.5 m (LOFAR)

- "Noise" by turbulent fields in a limited range of Faraday depths
- S/N > 2 sufficient to detect turbulent fields

Wavelet transformation of modeled magnetic fields

(Frick et al., A&A, in press, arXiv:1204.5694 (2012))

Regular fields ($h_{CR} > h_{th}$)

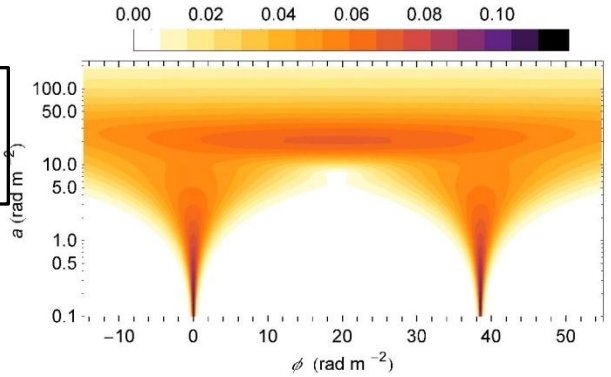

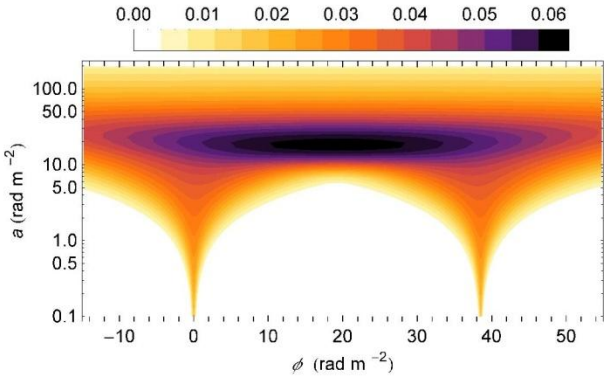

Regular fields ($h_{CR} = h_{th}$)

Regular fields (1 reversal)

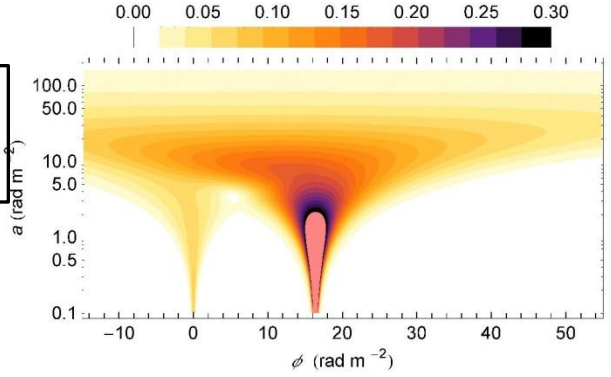

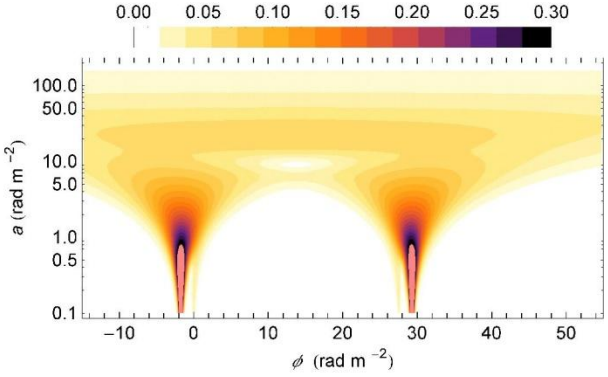

Regular fields (2 reversals)

Regular + turbulent fields

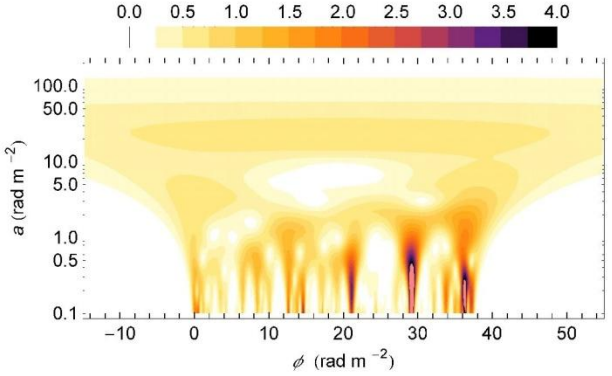

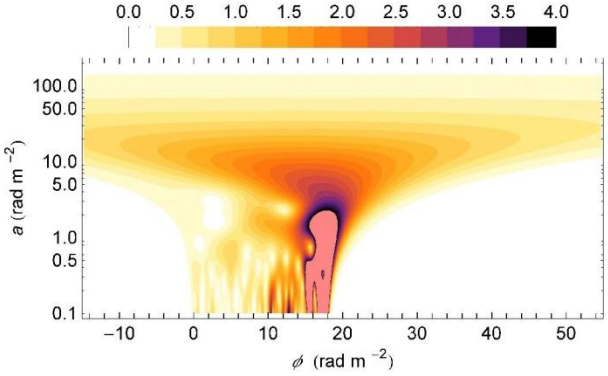

Regular field (1 reversal) + turbulent field

Present-day and future radio telescopes

(Frick et al. 2012)

FD resolution

FD scale

Telescope	λ (m)	$\Delta\lambda^2$ (m^2)	$\lvert\delta\phi\rvert$ (rad/m^2)	$\lvert\Delta\phi_{\rm max}\rvert$ (rad/m^2)	$(\lambda_{\rm max}/\lambda_{\rm min})^2$
LOFAR HBA	1.25–2.73	5.9	0.59	2.8	4.8
WSRT	0.17–0.23 + 0.77–0.97	0.91[1]	3.8	110	33
GMRT	0.21–0.30 + 0.47–0.52 + 0.87–0.98	0.92[1]	3.8	71	22
DRAO, Parkes, Effelsberg (GMIMS)	0.17–0.23 + 0.33–1.0	0.97	3.6	110	35
Parkes (S-PASS)	0.12–0.14	0.004	870	220	1.4
Arecibo (GALFACTS)	0.20–0.24	0.021	165	79	1.4
EVLA	0.025–0.30	0.089	39	5000	144
ATCA	0.03–0.27	0.072	48	3500	81
ASKAP (POSSUM)	0.21–0.27	0.026	130	71	1.6
(POSSUM + FLASH)	0.21–0.42	0.14	25	71	4.0
SKA Phase 1	0.10–4.3	18	0.19	310	1850
SKA Phase 2	0.03–4.3	18	0.19	3500	20500

Table 1. Spectral ranges of various radio telescopes and parameters crucial for wavelet-based RM Synthesis

[1] High sidelobes in Faraday spectrum expected due to the large gaps in wavelength coverage

Observation of regular magnetic fields

(Frick et al. 2012)

LOFAR

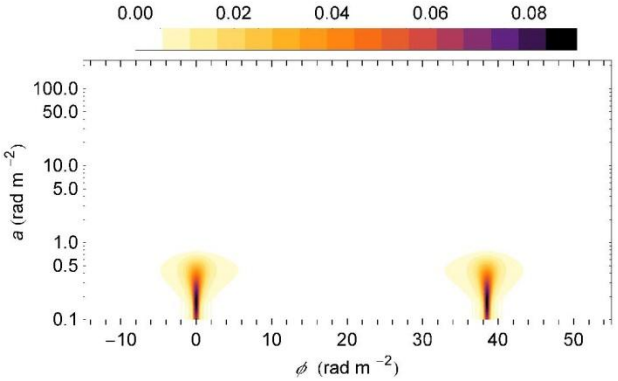

WSRT

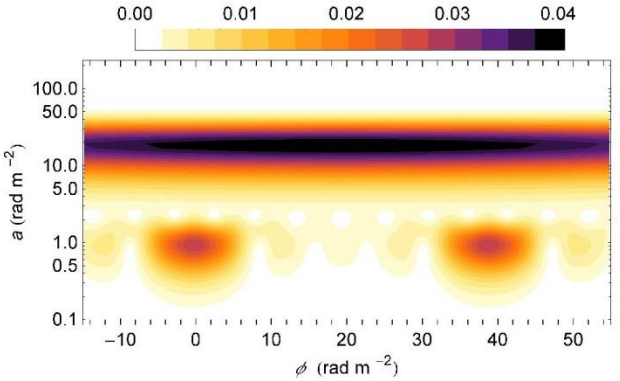

EVLA

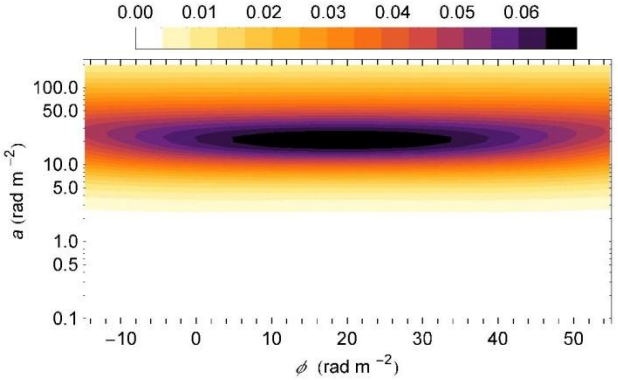

ASKAP (POSSUM)

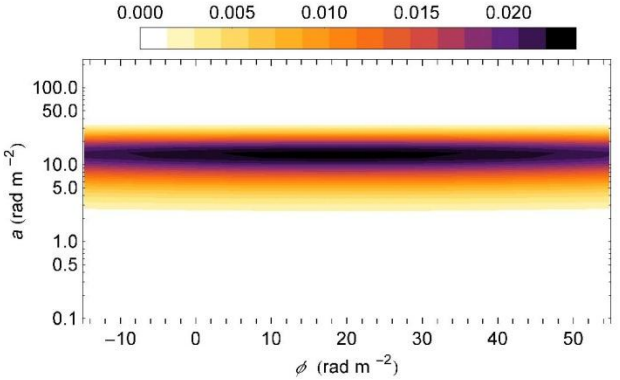

ASKAP (POSSUM + FLASH)

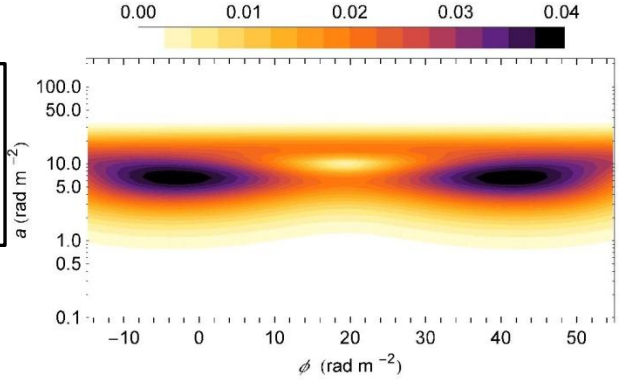

SKA Phase 1

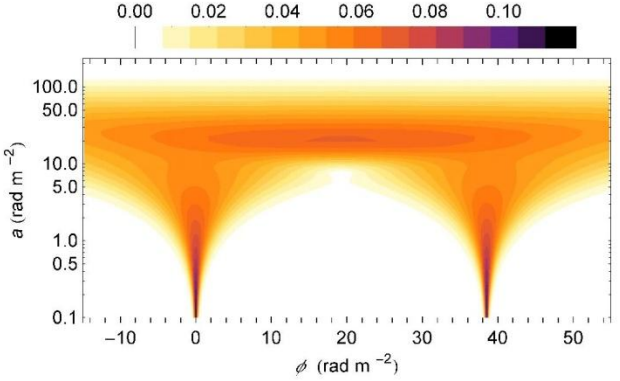

Observation of regular magnetic fields with one reversal

(Frick et al. 2012)

LOFAR

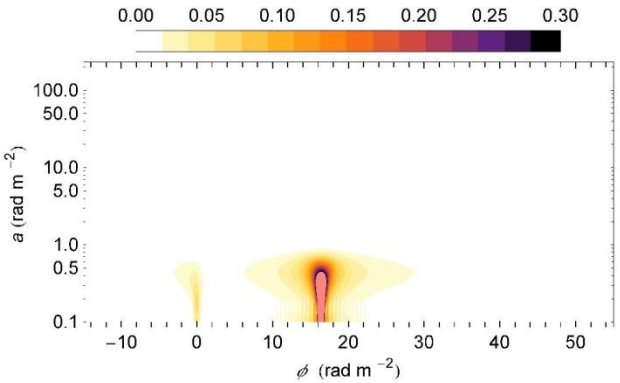

WSRT

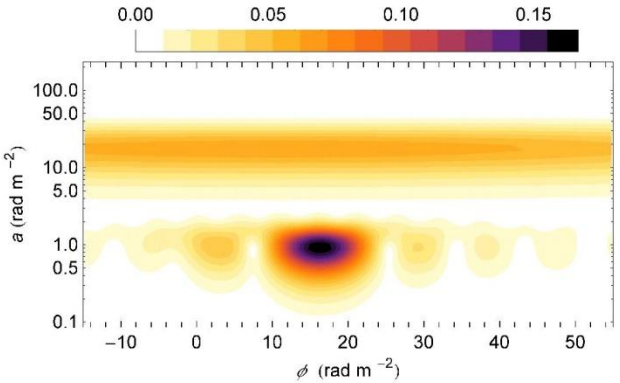

EVLA

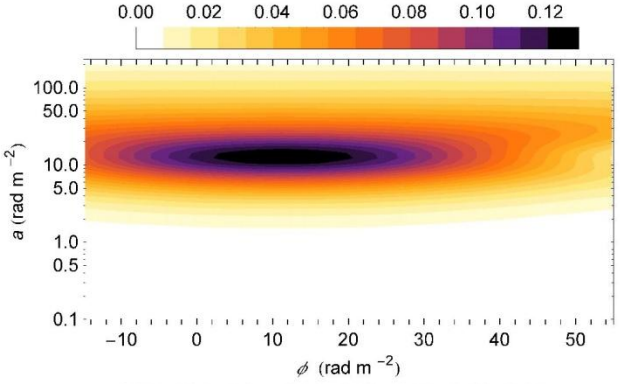

ASKAP (POSSUM)

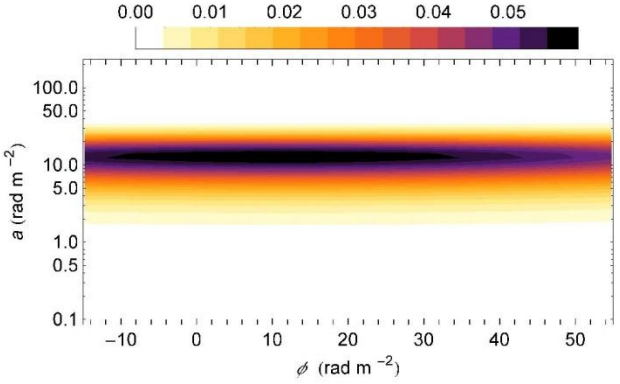

ASKAP (POSSUM + FLASH)

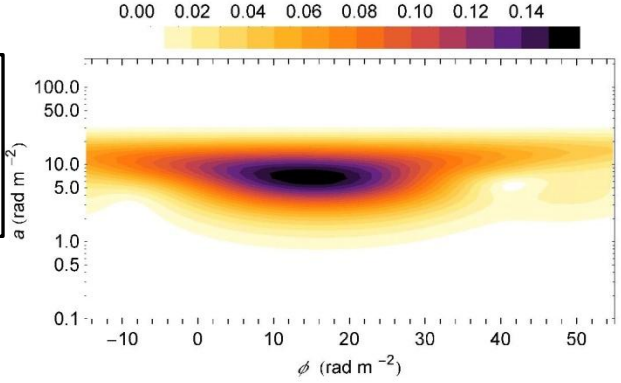

SKA Phase 1

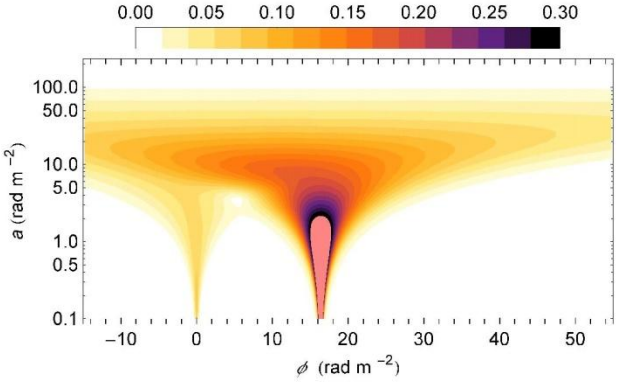

Observation of regular magnetic fields with two reversals

(Frick et al. 2012)

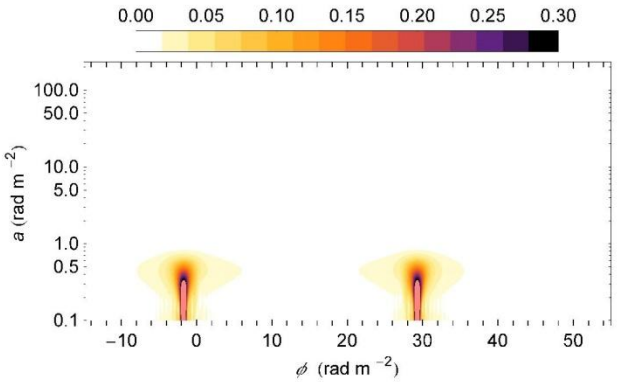

LOFAR

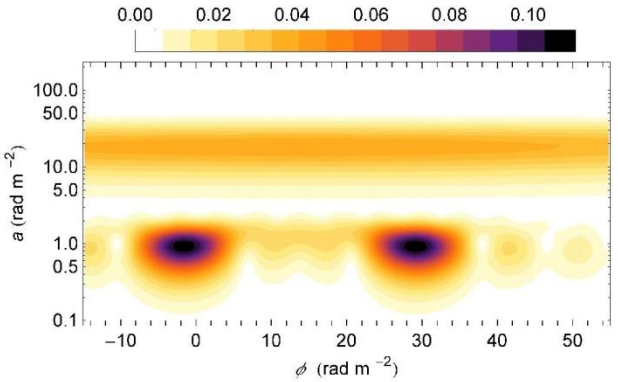

WSRT

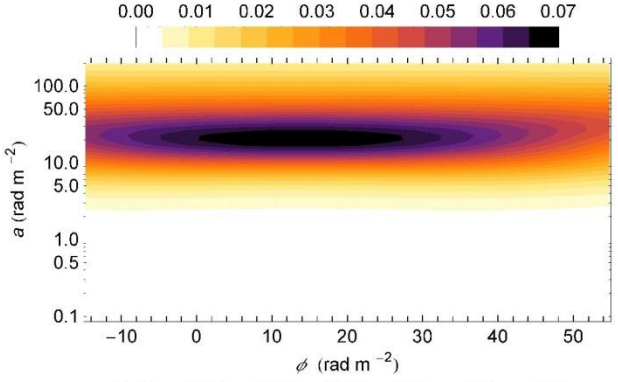

EVLA

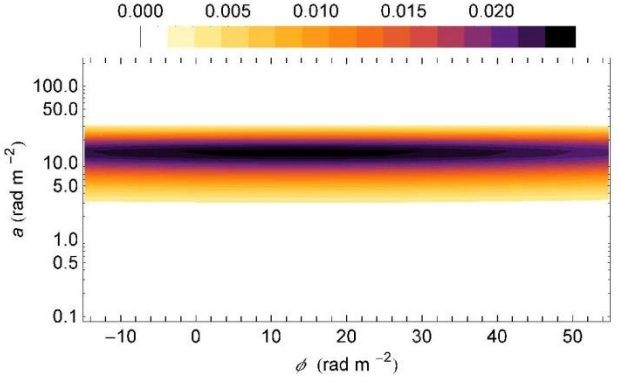

ASKAP (POSSUM)

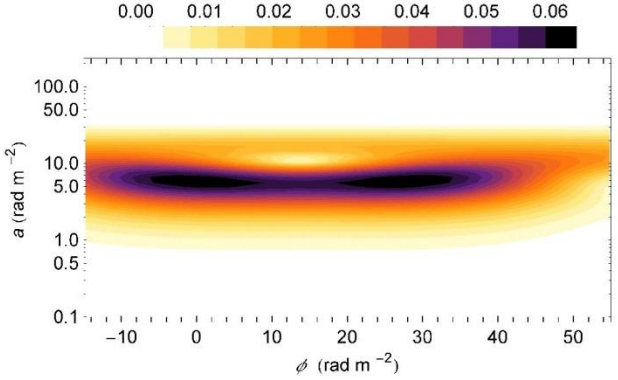

ASKAP (POSSUM + FLASH)

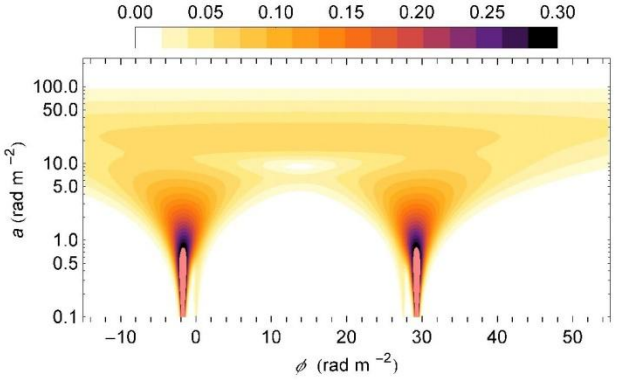

SKA Phase 1

Observation of regular + turbulent magnetic fields

(Frick et al. 2012)

LOFAR

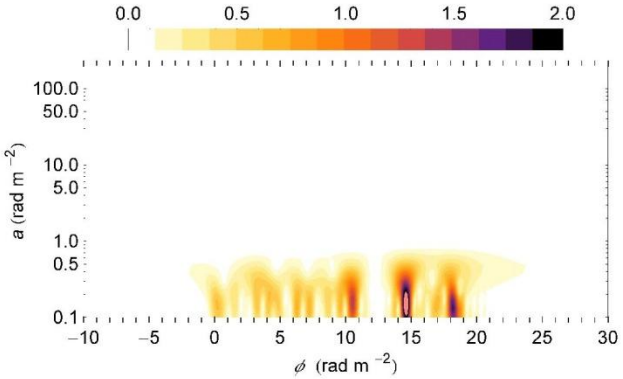

WSRT

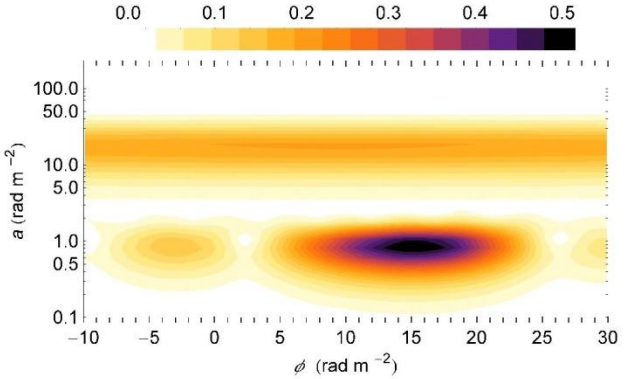

EVLA

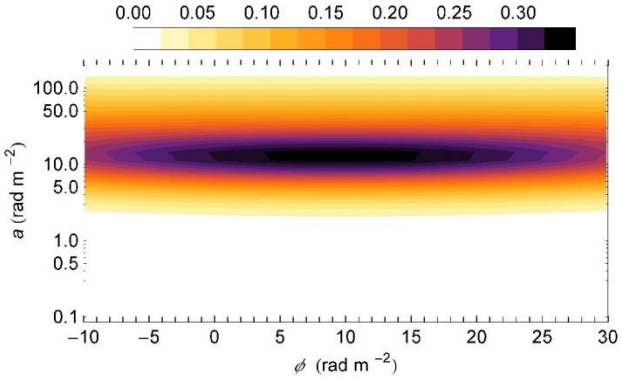

ASKAP (POSSUM)

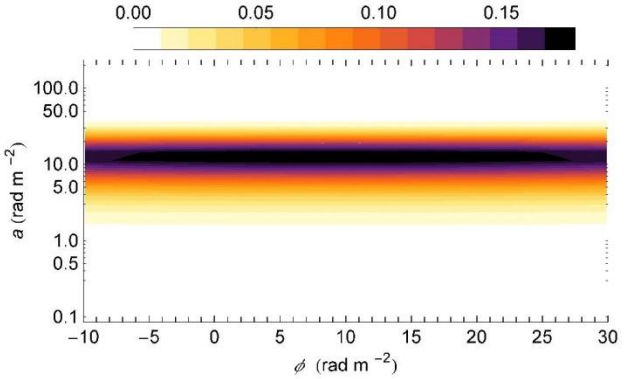

ASKAP (POSSUM + FLASH)

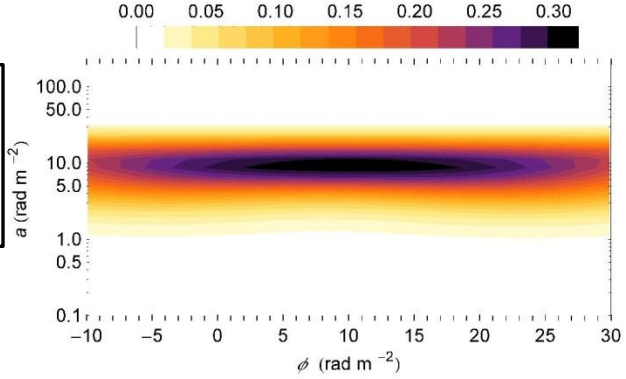

SKA Phase 1

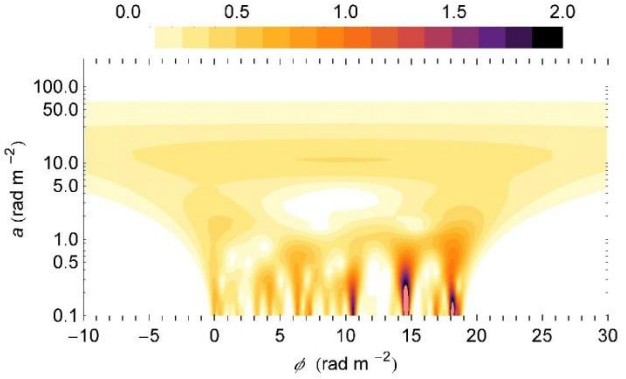

Conclusions

- Wavelet-based RM Synthesis can reconstruct complex features in Faraday spectra better than classical RM Synthesis

- Wavelet-based RM Synthesis is much better in reconstructing polarisation angles

- Wavelet-base RM Synthesis needs to be extended to 3-D

- Comparison of different methods of RM Synthesis is needed with help of standard models

- Comparison of processing times is needed

- Data representation with wavelets is helpful to analyze structures in Faraday space by measuring the composition of different scales